Nanoscale

Accepted Manuscript

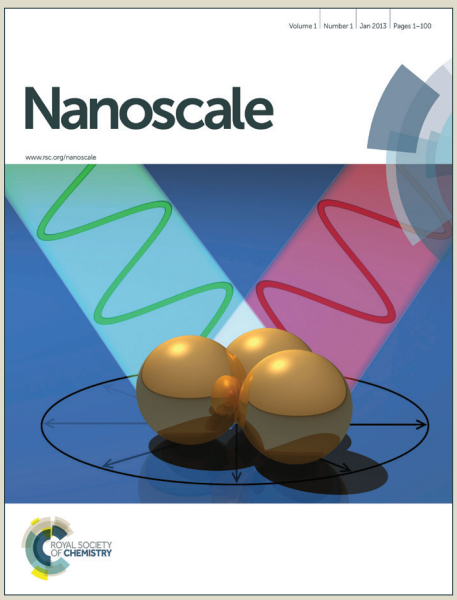

ROYAL SOCIETY OF CHEMISTRY

www.rsc.org/nanoscale

Journal Name

RSCPublishing

ARTICLE

Nd^{3+}-sensitized Upconversion Nanophosphor Modified with Cyanine Dye for Ratiometric Upconversion Luminescence Bioimaging of Hypochlorite

Cite this: DOI: 10.1039/xoxxoooooox

Received ooth January 2012,
Accepted ooth January 2012

DOI: 10.1039/xoxxoooooox

www.rsc.org/

Xianmei Zou,[a] Yi Liu,[a] Xingjun Zhu,[a] Min Chen,[a] Liming Yao,[a] Wei Feng,*[a] and Fuyou Li*[a]

Excessive or misplaced production of ClO^- in living systems is usually associated with many human diseases. Therefore, it is of great importance to develop an effective and sensitive method to detect ClO^- in living system. Herein, we designed an 808 nm excited upconversion luminescence nanosystem, composed of Nd^{3+}-sentitized core-shell upconversion nanophosphor $NaYF_4$:30%Yb,1%Nd,0.5%Er@$NaYF_4$:20%Nd, which serves as an energy donor and $HOCl^-$ responsible cyanine dye hCy3 which acts as an energy acceptor, for ratiometric upconversion luminescence (UCL) monitoring of ClO^-. The detection limit of ClO^- for this nanoprobe in aqueous solution is 27 ppb and the nanoprobe was successfully used to detect the ClO^- in the living cells by ratiometric upconversion luminescence. Importantly, the nanoprobe realized the detection of ClO^- in a mouse model of arthritis, which produced an excess of ROS, under 808 nm irradiation in vivo. The excitation laser efficiently reduced the heating effect, compared to the common used 980 nm laser for upconversion systems.

Introductions

Hypochlorous acid (HOCl) or hypochlorite (ClO^-) has received an increasing attention, because of its important role in animal immune systems, especially during phagocytosis.[1-5] The highly active hypochlorite can mediate the chemical modification of various biomolecules such as DNA, RNA, lipids and proteins, and then kill the invading pathogens.[6, 7] Excessive production of HOCl/ClO^- in living system is associated with many human diseases, including hepatic ischemia-reperfusion injury, atherosclerosis, lung injury, rheumatoid arthritis, and even cancers.[4, 8] Therefore, highly sensitive and selective detection of HOCl/ClO^- in living samples is vitally required.

Fluorescent bioimaging offers an available visualization approach to detect HOCl/ClO^-, because of its various advantages including high sensitivity and simplicity. To date, several HOCl/ClO^--sensitive fluorescence probes have been developed with a change in fluorescence intensity under the HOCl/ClO^--rich microenvironment.[5, 9-12] However, most available HOCl/ClO^--sensitive fluorescent probes required the usage of ultraviolet (UV) or visible light as the excitation resource, which causes a possible detrimental effect to healthy cells and organs. To overcome this problem, near-infrared (NIR)-excited organic dyes were also introduced for HOCl/ClO^- detection.[2, 13] However, the reported NIR-excited organic dyes have the disadvantages of easy photobleaching and small Stokes shift.

As an alternative of organic NIR dyes, lanthanide-doped upconversion nanophosphors (UCNPs), as new NIR-excited materials, show several advantages such as superior photostability, large anti-Stokes shift of several hundred nanometers, and no autofluorescence from biological specimens.[14-21] As a result, UCNPs have been successfully used in bioimaging and detection under NIR excitation.[22-27] In particular, using the UCNPs as energy donor to transfer energy to the organic chromophores (acceptors), several upconversion luminescence resonance energy-transfer (UC-LRET) or emitter-absorber systems have been successfully developed to detect specific ions,[28-31] DNA,[32-34] and small molecules.[35-38] Most of these reported UC-LRET systems were focused on lanthanide nanomaterials with Yb^{3+} as the sensitizer, and thus continuous-wave (CW) 980 nm laser was used as an excitation resource. Unfortunately, 980 nm light is strongly absorbed by water molecules in biological samples and can cause overheating effect, resulting in possible cell death and tissue damage.[39-41] To minimize the overheating effect, some research groups have recently utilized Nd^{3+} ion as sensitizer and the 808 nm laser as an alternative of the 980 nm excited light, because of the low absorption coefficient of water at 800 nm.[40, 42, 43] Although this $Nd^{3+}\rightarrow Yb^{3+}\rightarrow$activator energy transfer process under 800 nm

excitation can render effective upconversion performance, such Nd^{3+}-sensitized upconversion process has rarely been applied in further detection field.

Herein we designed and synthesized a Nd^{3+}-sensitized upconversion luminescence nanosystem (hCy3-csUCNPs:Nd, Scheme l) for ratiometric upconversion luminescence (UCL) probing of ClO^- under 808 nm irradiation with minimized heating effect. This nanosystem was composed of Nd^{3+}-sentitized core-shell upconversion nanophosphor $NaYF_4$:30%Yb,1%Nd,0.5%Er@$NaYF_4$:20%Nd (abbreviated as csUCNPs:Nd) as an energy donor, and ClO^--responsive cyanine dye hCy3 as an energy acceptor. Using the ratiometric UCL emission at 540 nm to 654 nm as the detection signal, hCy3-csUCNPs:Nd was successfully used as a high-contrast nanoprobe for probing ClO^- in living cells. Furthermore, the nanoprobe realized the detection of ClO^- in mouse model with arthritis in vivo.

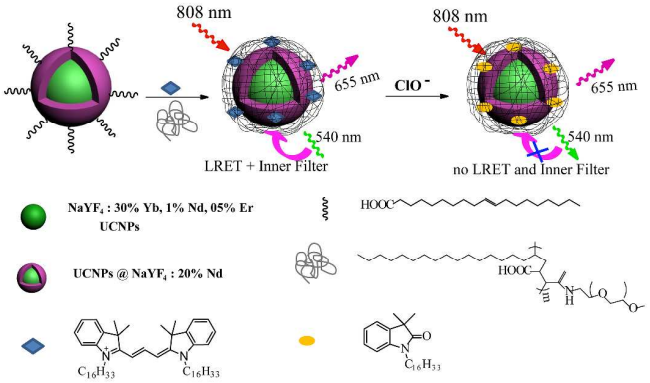

Scheme 1. Schematic illustration of the synthesis of hCy3-csUCNPs:Nd and its probing to ClO^- with a change in ratiometric UCL emission. The green UCL emission of csUCNPs:Nd is quenched due to the presence of hCy3 which has an absorption band at the corresponding wavelength. When ClO^- is added, the structure of hCy3 changed resulting in the absorption decreased and the green UCL emission is turned on.

Results and Discussion

Design and principle in upconversion detection process.

For lanthanide-doped UCNPs, there is no recognition unit in their surface, which limits their application in the field of detection. For the design of upconversion ClO^- probe, we constructed a system working with both inner filter effect and luminescence resonance energy transfer (LRET) process, with Nd^{3+}-sensitized upconversion nanophosphor as the energy donor and ClO^--sensitive chromophore (hCy3) as the acceptor (Scheme 1). Luminescence resonance energy transfer is a unique process to generate luminescence signal,[44] based on the overlap between the donor emission and acceptor excitation spectra. Thus, tuning the spectral overlap can change the donor emission. The inner filter effect has the similar spectra overlap requirement, thus this two kind of mechanism can work together in our system. Herein, $Nd^{3+} \rightarrow Yb^{3+} \rightarrow Er^{3+}$ upconversion emissions were used as detection signal, and a cyanine dye Cy3 derivative (hCy3) was chosen as energy acceptor. The broad absorption band peaks at 558 nm of hCy3 matched the UCL emissions of $^2H_{11/2} \rightarrow {}^4I_{15/2}$, $^4S_{3/2} \rightarrow {}^4I_{15/2}$ transition (λ_{UCL} = 514-530 nm and 530-560 nm) of Er^{3+}, meaning that the upconversion emission can be modulated with the addition of ClO^-.

Optical response of hCy3 to HOCl.

The responsive ability of hCy3 to NaClO was investigated in EtOH/phosphate buffer solution (1:1, v/v). Fig. 1 shows the absorption and fluorescence emission spectra of hCy3 in different concentration of NaClO. Upon addition of NaClO, the absorbance intensity of hCy3 at 558 nm ($\varepsilon = 1.3 \times 10^5\ M^{-1}\ cm^{-1}$) decreased gradually, leading to an evident color change (Fig. 1a inset), which indicated a reaction between hCy3 and NaClO. Because of its strong oxidation ability, ClO^- can react with the large-conjugated cyanine dyes to form corresponding oxindole and reduce its absorption.[45] At the concentration of hCy3 used in this study, the detection limit for ClO^- was ~103 ppb. Furthermore, the selectivity experiment indicated that very weak variations in absorption spectrum of hCy3 were observed upon addition of an excess of other analytes, such as m-CPBA, t-BuOOH, O^{2-}, H_2O_2, •OH, NO, $^1O_2$, and $ONOO^-$ (Fig. S6). These results indicated that hCy3 can serve as an excellent colormetric indicator for ClO^-. Unfortunately, the addition of NaClO to hCy3 resulted in a prominent emission decrease in 565 nm (Fig. 1), and such fluorescence turn-off probe can easily be interferred by detection environment.

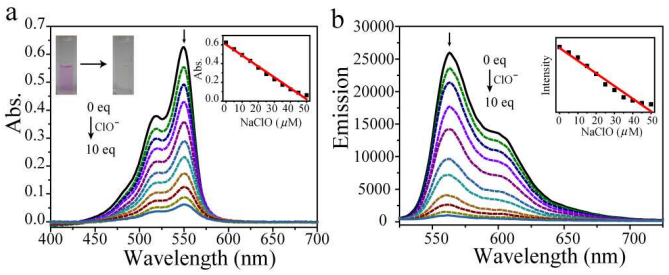

Fig. 1 (a) Changes in absorption spectra and fluorescence emission spectra (b) of 5 μM solution of hCy3 upon gradual addition of NaClO.

Synthesis and characteristics of Nd^{3+}-sensitized UCNPs.

To enhance the Nd^{3+}-sensitized upconversion emission of Er^{3+}, a core-shell nanophosphor (abbreviated as csUCNPs:Nd) composed of the core of $NaYF_4$:30%Yb,1%Nd,0.5%Er and the shell layer of $NaYF_4$:20%Nd was designed. The OA-coated hexagonal-phased csUCNPs:Nd were synthesized through epitaxial growth[46] of $NaYF_4$:Nd shells onto $NaYF_4$:Yb,Nd,Er cores. As characterized by transmission electron microscopy (TEM), the core nanoparticle (OA-$NaYF_4$:Yb,Er,Nd) had a spherical shape with an average size of ~18 nm (Fig. 2a, 2b). After the $NaYF_4$:Nd (20%) layer was coated onto the surface of the core nanoparticles, the average size of csUCNPs:Nd was

increased to ~24 nm (Fig. 2c, 2d). The core-shell nanostructure was also confirmed by the results change in the energy-dispersive X-ray analysis (EDXA) as shown in Fig. S7 with the increasing of the concentration of Nd. Under CW excitation at 808 nm, csUCNPs:Nd displayed three obvious upconversion emission bands at 514-530 nm, 530-560 nm and 630-670 nm. However, the upconversion emission of the core-shell nanocrystals was significantly enhanced compared to that of the core alone. (Fig. S8).

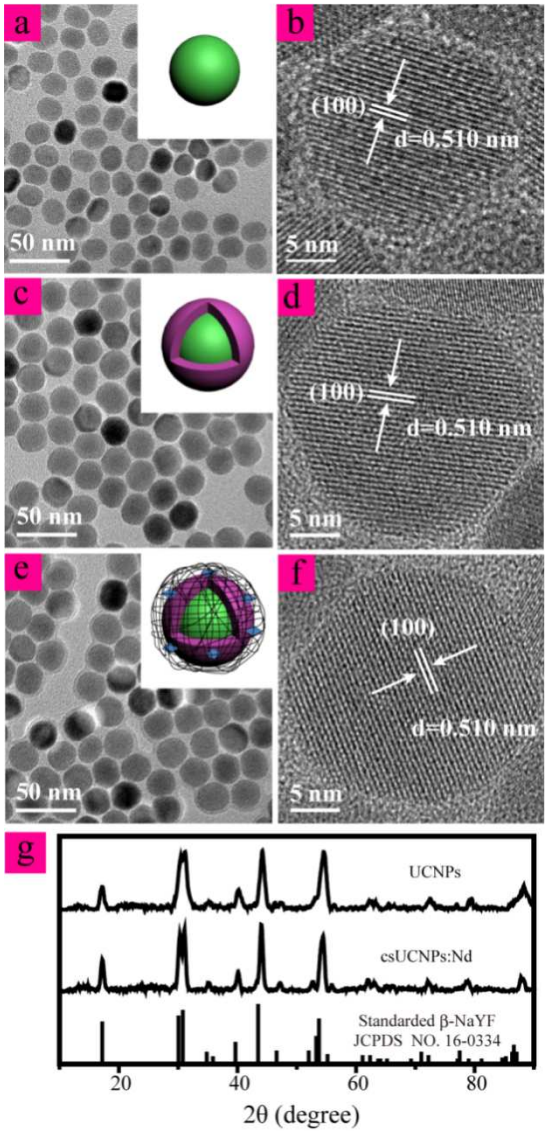

Fig. 2 TEM (a) and HR-TEM (b) images of OA-UCNPs. TEM (c) and HR-TEM (d) images of csUCNPs:Nd. TEM (e) and HR-TEM (f) images of hCy3-csUCNPs:Nd. (g) X-ray diffraction pattern of UCNPs and csUCNPs:Nd. The standard pattern of β-$NaYF_4$ (JCPDS no.16-0334) is also shown.

The upconversion emission spectrum of csUCNPs:Nd was compared together with the absorption spectra of hCy3 in Fig. 3. The absorption band of hCy3 (450-580 nm) matched well with the green UCL emission of transition bands of Er^{3+}, which means inner filter effect and LRET process can exist to quench the green emission of csUCNPs:Nd. In combination with the modulation in absorption band of hCy3 at 558 nm by ClO^- addition, ClO^- can tune the Nd^{3+}-sensitized green upconversion emission of Er^{3+}. Meanwhile, due to the few overlap between the red emission of csUCNPs:Nd and absorption band of hCy3, the red UCL emission was not influenced by ClO^- and can be taken as a reference to allow ratiometric upconversion detection.

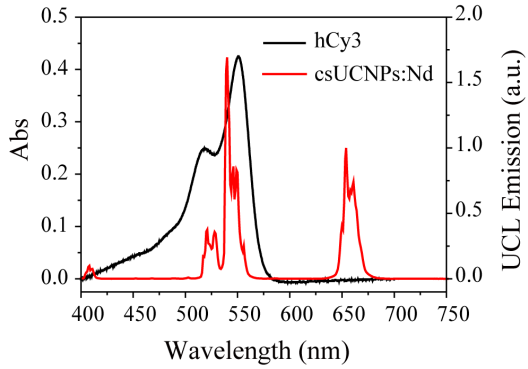

Fig. 3 UCL emission spectra of csUCNPs:Nd and the UV-vis absorption spectra of hCy3.

Synthesis and characterization of the nanosystem hCy3-csUCNPs:Nd

In order to obtain a water-soluble nanosystem composed of both the csUCNPs:Nd and the acceptor hCy3, the amphiphilic polymer p-PEG (Scheme 1) and hydrophobic hCy3 were cooperatively modified on the surface of the csUCNPs:Nd through a hydrophobic-hydrophobic interaction. The hCy3-csUCNPs:Nd could be well-dispersed in water for more than six months, whereas the csUCNPs:Nd was well-dispersed in cyclohexane, indicating successful coating of p-PEG on the csUCNPs:Nd particle's surface. TEM images showed that p-PEG coating has no significant changes in shape of csUCNPs:Nd (Fig. 2e-2f). The X-ray diffraction peaks of UCNPs and csUCNPs:Nd were well indexed to the hexagonal phase $NaYF_4$ (JCPDS NO.16-0334), which was also confirmed by the high-resolution transmission electron microcopy (HR-TEM) image (Fig. 2g).

The assembly of the amphiphilic polymer p-PEG and organic probe hCy3 on the csUCNPs:Nd surface was further confirmed by Fourier-transform infrared (FTIR) spectroscopy. In the FTIR spectrum of OA-csUCNPs:Nd (Fig. S9), the peaks at 2927 and 2855 cm^{-1} were attributed to the asymmetric and symmetric stretching vibrations of methylene (-CH_2-) in the long alkyl chain. The bands at 1567 cm^{-1} were assigned to δ(C=O), indicating that OA was coated on the surface of the nanoparticles. Compared with the spectrum of OA-UCNPs:Nd, new peaks at 2922, 2959, 1557, and 1157 cm^{-1} were attributed to the p-PEG and hCy3 appearing in hCy3-csUCNPs:Nd, which confirmed the successful assembling of p-PEG and hCy3 on the surface of OA-csUCNPs:Nd. Subsequently, the amount of loaded hCy3 in the nanosystem was measured to be about 12.0% by a UV-Vis absorption analysis (Fig. S10). Therefore,

after the polymer self-assembly process, a water-soluble three-layer structure nanosystem (hCy3-csUCNPs:Nd, Scheme 1) composed of an inner core of csUCNP:Nd, a middle layer containing ClO^--sensitive hCy3, and outside hydrophilic layer of p-PEG was created. Under excitation at 808 nm, three main upconversion emission bands at 514-530 nm, 530-560 nm and 630-670 nm originated from Er^{3+} were still observed for hCy3-csUCNPs:Nd nanosystem in aqueous solution (Fig. 4). Compared with the UCL emission spectrum of p-PEG modified OA-csUCNPs:Nd shown in Fig. 3, the green UCL intensity of hCy3-csUCNPs:Nd decreased by 81.3%. Deduced from the corresponding absoption spectra, the inner filter effect contributed 73.1% decrease, while the LRET efficency was 30.5%. At the same time, a new weak upconversion emission band peaks at 575 nm which matched the Stokes fluorescence emission of hCy3 was also observed. The appearance of this new UCL band confirmed the LRET process between csUCNPs:Nd and hCy3.

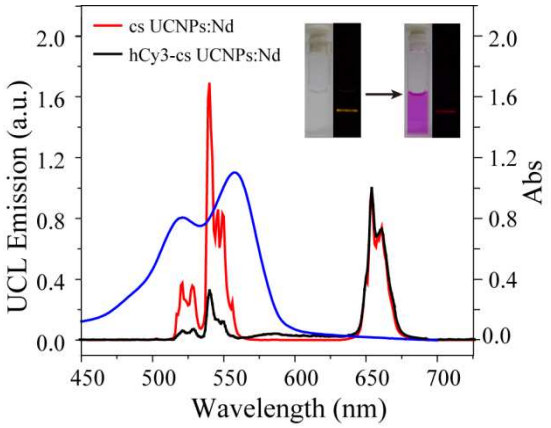

Fig. 4 UV-vis Absorption spectrum (blue line) of hCy3-csUCNPs:Nd and UCL emission spectra of csUCNPs:Nd (red line) and hCy3-csUCNPs:Nd (black line) under excitation at 808 nm.

Probing of hCy3-csUCNPs:Nd for NaClO

The responsive ability of hCy3-csUCNPs:Nd for NaClO was further investigated (Fig. 5). In the UV-Vis absorption spectrum, the hCy3-csUCNPs:Nd exhibited a broad visible absorption band with the maximum wavelength at 558 nm. The absorbance reduced linearly when increasing the amount of NaClO in the range of 0 to 80 μM, indicating that hCy3 in the middle layer reacted with NaClO. This also affected the upconversion emission signals by the inner filter effect and LRET process. As shown in Fig. 5b, the intensity of green UCL emission of hCy3-csUCNPs:Nd at 514-530 nm and 530-560 nm were gradually increased following addition of the amounts of NaClO. It was attributed to the reduced of spectral overlap between the absorption (λ_{abs} = 450-580 nm) of hCy3 and green UCL emission (λ_{em} = 514-560 nm) of csUCNPs:Nd upon addition of NaClO. Moreover, addition of NaClO caused almost no effect to the UCL emission peaks at 654 nm under excitation at 808 nm. Thus, the ratio of UCL emission intensity at 540 nm to 654 nm can be taken as detection signal. The UCL ratio ($UCL_{540\ nm}$ / $UCL_{654\ nm}$) versus the addition amount of NaClO is shown as inset in Fig. 5b. The ratio of UCL intensity increased linearly with the NaClO concentration from 0 to 80 μM. Generally, compared with the emission intensity detection, the ratiometric method applied avoids the influence of change in concentration or other factors in the test procedure. Using the ratiometric UCL detection, the detection limit of hCy3-csUCNPs:Nd for NaClO in aqueous solution was measured to be 27 ppb (~0.5 μM), which was significantly lower than that (~103 ppb) of absorption method and reaches the physiological concentration (5-200 μM) of hypochlorite. Such a high sensitivity of ratiometric UCL detection of ClO^- should be attributed to low background signal in upconversion technique.

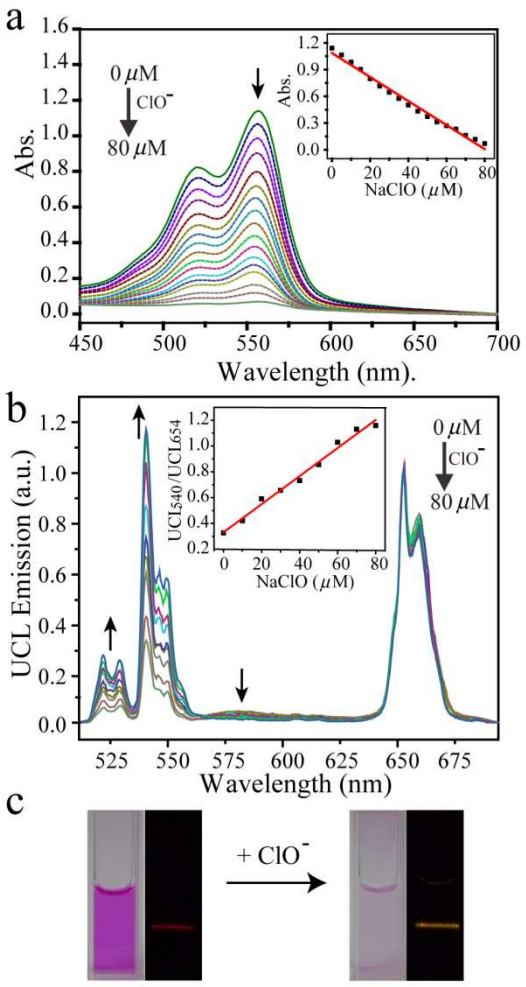

Fig. 5 (a) The UV-vis absorption spectra of 0.1 mg/mL hCy3-csUCNPs:Nd in aqueous solution upon gradual addition of NaClO and the absorbance intensity at 550 nm as a function of NaClO concentration (inset). (b) Upconversion luminescence spectra of 0.1 mg/mL hCy3-csUCNP:Nd under 808 nm irradiation in aqueous solution upon gradual addition of NaClO (from 0 to 80 μM) and the ratio of the UCL emission at 540 nm to 654 nm as a function of NaClO concentration (inset). (c) Photoluminescence spectra changes of the hCy3-cs UCNPs:Nd upon addition of ClO-.

For an excellent detection nanosystem, high selectivity is very important. To validate the selectivity of hCy3-csUCNPs:Nd, its UCL emission response to various biologically relevant species reactive oxygen species (ROS) were also investigated under the same condition. As shown in Fig. 6, addition of other ROS and RNS species, including m-CPBA, t-BuOOH, O^{2-}, H_2O_2, •OH, NO, $^1O_2$, or $ONOO^-$, did not cause obvious enhancement of green UCL emission and significant color changes (Fig. 6c). These facts indicated that the present nanosystem hCy3-csUCNPs:Nd can specifically detect ClO^- over other ROS and RNS species.

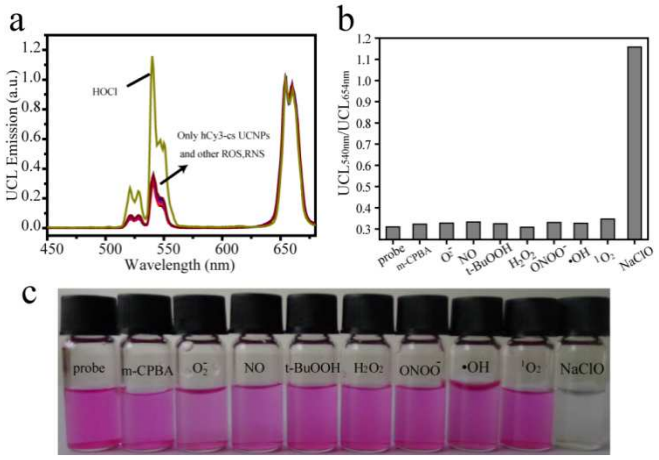

Fig. 6 (a) UCL emission spectra of hCy3-csUCNPs:Nd (0.1 mg/mL) with various ROS and RNS species under the same condition. (b) Ratiometric UCL responses ($UCL_{540\ nm}/UCL_{654\ nm}$) of hCy3-csUCNPs:Nd with various ROS species. (c) The photograph of color changes upon addition of various ROS species.

Cytotoxicity assessments

Before further cell and animal experiments, the cytotoxicity of hCy3-csUCNPs:Nd was investigated by a standard methyl thiazolyl tetrazolium (MTT) assay (Fig. 7). It was shown that more than 90% of the cells can survive even after incubation of hCy3-csUCNPs:Nd with an extremely high concentration (600 μg/mL) for 24 h and 48 h, demonstrating the low cytotoxicity of hCy3-csUCNPs:Nd.

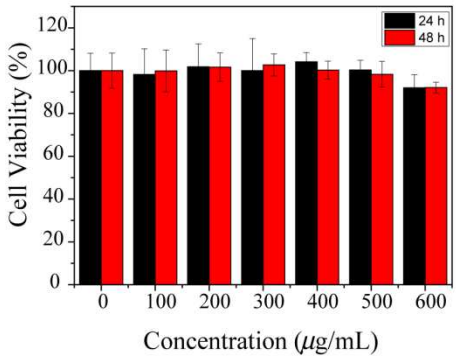

Fig. 7 In vitro cell viability of HeLa cells incubated with hCy3-csUCNPs:Nd at different concentration for 24 and 48 hours.

Probing NaClO in living cells

By utilizing a laser scanning upconversion luminescence microscopy under CW excitation at 808 nm, further practical application of hCy3-csUCNPs:Nd in probing intracellular ClO^- was investigated (Fig. 8). HeLa cells incubated with hCy3-csUCNPs:Nd for 4 h at 37 °C showed a weak green UCL emission and relative intense red UCL signal (Fig. 8b and 8c). After the cells were supplied with 5 μM NaClO in the growth medium for 30 min at 37 °C and then incubated with hCy3-csUCNPs:Nd under the same conditions, a strong enhancement in the green UCL emission was observed in the intracellular region (Fig. 8g). Furthermore, the ratiometric UCL imaging was further carried out when the UCL ratio at the green channel (λ_{UCL} = 500-560 nm) to red channel (λ_{UCL} = 600-700 nm) was used as the detection signal. As shown in Fig. 8e, HeLa cells incubated with hCy3-csUCNPs:Nd (350 μg/mL) for 4 h at 37 °C showed a UCL ratio of <0.4. For the NaClO pretreated HeLa cells incubated further with hCy3-csUCNPs:Nd (350 μg/mL), the corresponding UCL ratio was increase to 0.85 under the same condition (Fig. 8j). This results confirmed that hCy3-csUCNPs:Nd can be used to probe intracellular NaClO with the ratiometric UCL imaging.

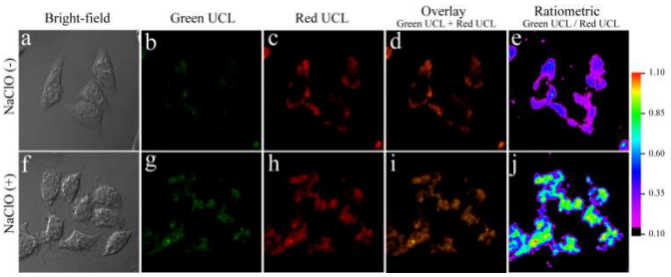

Fig. 8 Ratiometric UCL images in living HeLa cells (top, a-e) and 5 μM NaClO-pretreated Hela Cells (bottom, f-j) incubated with 350 μg/mL hCy3-csUCNPs:Nd for 4 h at 37 °C. Emission was collected by green UCL channel at 500-560 nm (b and g) and red channel at 600-700 nm (c and h). (d and i) Overlay of green UCL and red UCL images. (e and j). Ratiometric UCL images with ratio of green to red channels.

In vivo imaging of physiological HClO production

To test whether the nanosystem (hCy3-csUCNPs:Nd) can be used as specific fluorescent probe for the detection of physiological HOCl production in vivo, we applied it in a mouse model of arthritis, that is a well-known HClO producing disease. The arthritis was induced by injecting 50 μL λ-carrageenan (10 mg/mL, in 0.9% NaCl) into the left tibiotarsal ankles of 4-week-old mouse, and the right tibiotarsal ankles of the same mouse were injected with the same volume of physiological saline as control group. After four hours, the arthritis was successfully induced in the left leg (Fig. S12) and then the left and right ankles were injected with the same amount of hCy3-csUCNPs:Nd. The UCL imaging in vivo was shown in figure 9. Compared with control group treated with normal saline, the UCL of green emission increase 2 times in the left inflammation parts under 808 nm irradiation. This

findings indicated that the nanosystem can detect arthritis-dependent HClO production in vivo.

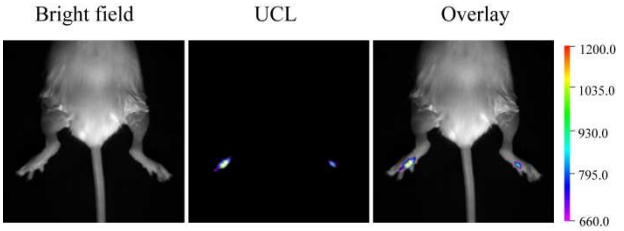

Fig. 9 In vivo UCL images of the arthritis living mouse with injection of 50 uL hCy3-csUCNPs:Nd in left leg and right leg ankles under excitation power density of 400 mW cm^{-2}. (λ_{ex} = 808 nm, λ_{UCL} = 530±25 nm).

Heating Effect Evaluation.

In the reported long-term upconversion monitoring with 980 nm excitation, an overheating effect usually appeared. Herein, for hCy3-csUCNPs, a new upconversion probe, the heating effect was carried out on a model of nude mouse, using 808 nm and 980 nm lasers as the excitation resource. With the same power density of 400 mW/cm^2 for the lasers, the temperature change was monitored with an infrared thermal imager. A notable local heating effect and significant rise in temperature (Fig. S13) were observed under irradiation of the 980 nm laser for 300 s. In contrast, for the 808 nm laser irradiation, only a slight rise in temperature was observed within the same irradiation time. These facts indicated that 808 nm excitation showed a lower heating effect in animal UCL bioimaging compared to 980 nm excitation.

Conclusions

In summary, we designed and synthesized a three-layer core-shell nanosystem (hCy3-csUCNPs:Nd) composed of an inner core of Nd^{3+}-sensitized upconversion nanophosphors (csUCNPs:Nd), a middle layer containing ClO^--sensitive hCy3, and outside hydrophilic layer of p-PEG for highly sensitive and selective detection of ClO^-. The core-shell nanophosphors $NaYF_4$:Yb,Nd,Er@$NaYF_4$:Nd showed stronger UCL emission compared to the sole core $NaYF_4$:Yb,Nd,Er. The hCy3-csUCNPs:Nd nanosystem can detect ClO^- with low detection limit of 27 ppb, high selectivity and rapid response. This system was further successfully used to detect ClO^- in the living cells by ratiometric upconversion luminescence imaging. Importantly, the nanoprobe realized the detection of HClO in vivo mouse model of arthritis with the excitation laser at 808 nm wich efficiently eliminated the heating effect. Table 1 shows the specific features of our probe compared with those of others. We believe that this nanosystem can be used in many practical applications in biological systems.

Structure	Solvent	LOD	pH	λ_{ex}/nm	λ_{em}/nm	Comments	Reference
hCy3-UCNPs	H_2O	27 ppb (~0.5 μM)	7.0	808	540/655	Turn−on ratiometric fluorescent probe, in vitro and in vivo UCL detection	Our probe
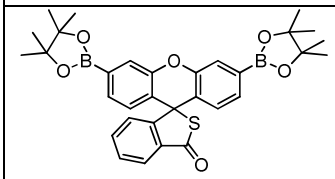	KH_2PO_4	0.2 μM	7.4	498	523	Turn−on fluorescent probe, high selectivity, sensitivity, short response time in a broad range of pH(5.5-9.3)	5
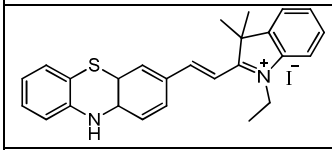	H_2O	0.836 μM	7.0	340	595	An absorbance ratiometric and a fluorescent off-on sensor, high sensitivity and selectively detect hROS	12
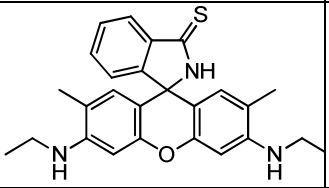	Ethanol/ H_2O (1/8, v/v)	1.07×10^{-8} M	6.5	520	563	Turn-on fluorescent chemodosimeter, remarkable fluorescent enhancement	49
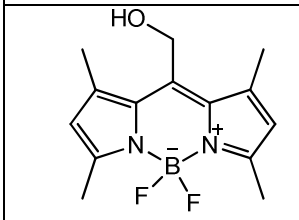	DMSO−HEPES buffer (1/99, v/v)	−	7.2	480	525	High specific, rapid turn-off response for HOCl in living cells	50

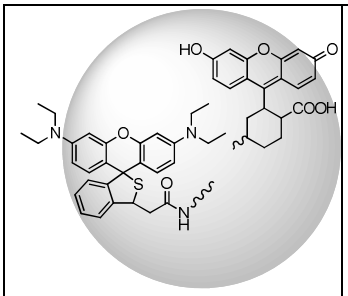	$Na_2HPO_4^{-}$ citrate buffer	5 μM	5.0	490	586	High selectivity, FRET based ratiometric detection of HOCl in living cells	51
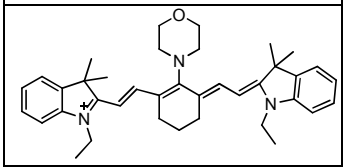	DMF/PBS (0.5/99.5, v/v)	1.95×10^{-8} M	7.4	540	566/780	High sensitive and selective, ratiometric imaging of HOCl in living cells	52
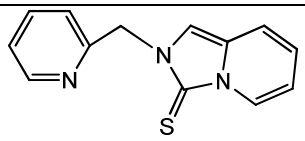	PBS/EtOH (3/1, v/v)	0.27 μM	7.4	365	430/505	Rapid and ratiometric sensor, high sensitivity and selectivity, bioimaging of HOCl in living cell	53

Table 1. Figures of merit of comparable methods for for the fluorometric determination and imaging of hypochlorite

Experimental section

Materials and methods

All reagents and chemicals were obtained from commercial supplies and used as received. Rare-earth oxides Y_2O_3(99.999%), Yb_2O_3 (99.999%) , Er_2O_3 (99.999%), and Nd_2O_3(99.999%) were purchased from Shanghai Yuelong New materials Co. Ltd. $RECl_3$ (RE^{3+}= Y^{3+}, Yb^{3+}, Er^{3+}, and Nd^{3+}) were prepared by dissolving the corresponding oxides in 10% HCl solution and then evaporating the water completely. Oleic acid (OA), 1-octadecane (ODE 90%) were obtained from Alrich. 3,3-dimethyl-3H-indole, 1-bromhexadecan,toluene, N,N'-diphenylforma-midine, AcOK, acetic anhydride , cyclohexanone, were obtained from Alfa Aesar Ltd. The amphiphilic block-polymer poly(maleic anhydride-alt-1-octadecene)-PEG (p-PEG) was prepared according to the previous literatures.

The size and morphology of UCNPs were determined at 200 KV using a JEOL JEM-2010F low to high resolution transmission electron microscope (TEM). The samples were dispersed in cyclohexane and dropped on the surface of a copper grid. Powder X-ray diffraction (XRD) measurements were performed on a Bruker D_4 diffractometer at a scanning rate of 1° /min in the 2θ range from 10 to 90° (Cu Kα radiation, λ=1.54056 Å). FT-IR spectra were measured using an IR Prestige-21 spectrometer (Shimadzu) from samples in KBr pellets. UV-vis absorption spectra were recorded on a Shimadzu 3000 spectrophotometer. UCL emission spectra were measured on an Edinburgh FLS920 luminescence spectrometer with an external 0-1.5W adjustable CW semiconductor laser at 808 nm (Shanghai Hi-Tech Optoelectronic Co., China). The ^{1}H NMR spectra were recorded on a Brucker spectrometer at 400 MHz. All chemical shifts were reported in the standard δ notation of parts per million. Electrospray ionization mass spectra were measured on a Micromass LCTTM system.

Synthesis of compound 2[47]

2,3,3-trimethylindolenine (3.20 g, 20.0 mmol) and 1-bromhexadecan (7.32 g, 24.0 mmol) were dissolved in toluene (30 ml). The solution was refluxed for 24 hours, and then was cooled to room temperature. The resulting solid was collected by filtration. The solid was washed with n-hexane and dried under reduced pressure to afford compound 2 as a red solid. MS (MALDI-TOF-MS): calcd. For $C_{27}H_{46}N^+$ 384.36 $[M]^+$; found 384.3141 $[M]^+$

Synthesis of compound hCy3

Compound 2 (4.64 g, 10.0 mmol), N,N'-diphenylformamidine (0.98 g, 5.0 mmol), and AcOK (0.97 g, 10.0 mmol) was dissolved in acetic anhydride (20 ml). The mixture was heated at 50 ˚C for about 30 min until the solution turned red, and then 100 mL H_2O was poured into the flask, and vigorous stirred for 10 min at room temperature. The mixture was filtered, and the crude dye was washed exhaustively with H_2O and ethyl ether for 3 times. The compound hCy3 was purified by silica column chromatography using DCM/MeOH (v/v, 40:1) mixture as eluent. The red fraction was collected, yielding small dye particles.^{1}H NMR (400 MHz, MeOD) δ 8.55 (t, J= 13.4 Hz, 1H), 7.55 (d, J= 7.1 Hz, 2H), 7.51 – 7.41 (m, 2H), 7.41 – 7.27 (m,4H), 6.47 (d, J= 13.5 Hz, 2H), 4.16 (t, J= 7.4 Hz, 4H), 1.85 (dt, J= 15.2, 7.6 Hz, 4H), 1.77 (s, 12H), 1.51 – 1.39 (m, 8H), 1.26 (s, 44H), 0.89 (t, J= 6.9 Hz, 6H). MS (MALDI-TOF-MS): calcd. For $C_{55}H_{89}N^+$ 777.70 $[M]^+$; found 777.7055 $[M]^+$.

Synthesis of Oleic Acid (OA)-Capped $NaYF_4$:Yb, Er, Nd (denoted as OA-UCNPs)

NaYF4:Yb,Er,Nd nanoparticles were prepared with a solvothermal method.[48] Typically, YCl_3 (0.685 mmol), $YbCl_3$ (0.30 mmol), $ErCl_3$ (0.005 mmol) and $NdCl_3$(0.01 mmol) were mixed with 6 mL oleic acid and 15 mL octadecene (ODE) in a 100 mL flask. The solution was heated to 140 °C to form lanthanide oleate complexes, and then cooled down to room temperature. Subsequenty, 8 mL methanol solution containing NaOH (2.5 mmol) and NH_4F (4 mmol) was added into the flask and stirred for 30 minutes. The temperature was then increased to 100 °C to remove the methanol from the reaction mixture, and then heated to 300 °C and maintained for 1 h under Ar protection. After the solution was cooled naturally, nanoparticles were precipitated from the solution with ethanol, collected by centrifugation, washed with ethanol and cyclohexane several times and finally redispersed in cyclohexane.

Synthesis of Oleic Acid (OA) Coated Core-shell $NaYF_4$:Yb,Nd,Er@$NaYF_4$:Nd (denoted as OA-csUCNPs:Nd)

Similarly, OA-csUCNPs:Nd core-shell nanoparticles were synthesized through epitaxial growth.[46] YCl_3 (0.40 mmol), $NdCl_3$ (0.10 mmol), were mixed with 6 mL oleic acid and 15 mL octadecene (ODE) in a 100 mL flask. The solution was heated to 140 °C to form a homogeneous solution, and then cooled down to 50 °C. The as-synthesized $NaYF_4$:Yb,Nd.Er nanoparticles in 5 mL of cyclohexane was added along with a 8 mL methanol solution containing NaOH (2.5 mmol) and NH_4F (4 mmol) The resulting mixture was stirred at 50 °C for 30 min. After the reaction temperature was increased to 100 °C to remove methanol, the mixture was heated to 300 °C and maintained for 1 h under Ar protection. After the solution was cooled naturally, nanoparticles were precipitated from the solution with ethanol, collected by centrifugation, washed with enthol and cyclohexane several times and finally redispersed in cyclohexane.

Assembly of p-PEG and hCy3 (denoted as hCy3-csUCNPs:Nd)

hCy3-csUCNPs:Nd were prepared according to the previous method.[31] The csUCNPs:Nd (10 mg) was dispersed in the 5 mL chloroform by ultrasonication, and then the mixture was stirred at room temperature to obtain a homogeneous phase. Furthermore, the amphiphilic polymer (p-PEG, 10 mg) was added, and then the mixture was stirred overnight at room temperature. The mixture was centrifugated (14000 rpm, 8 min every time in 20 °C), and the collected solid was repeatedly washed with water. The precipitate can be redispersed in deionized water.

Cell Culture

HeLa cells were cultured at 37 °C and 5% CO_2 in Dulbecco's Modified Eagle Medium (DMEM) supplemented with 10% fetal bovine serum (FBS), 1% penicillin / streptomycin.

Cytotoxicity of hCy3-csUCNPs:Nd

In vitro cytotoxicity was measured by performing methyl thiazolyl tetrazolium (MTT) assay on HeLa cells. Cells were seeded into a 96-well cell culture plate at 5×10^4 / well, under 100% humidity, and were cultured at 37 °C and 5% CO_2 for 24 h; different concentrations of hCy3-csUCNPs:Nd (0, 100, 200, 300, 400, 500 and 600 μg/mL, diluted in RPMI 1640) were then added to the wells. The cells were subsequently incubated for 24 h or 48 h at 37 °C under 5% CO_2. Then, MTT (10 μL; 5 mg/mL) was added to each well and the plate was incubated for an additional 4 h at 37 °C under 5% CO_2. After the addition of 100 μL DMSO, the assay plate was allowed to stand at room temperature for 2 h. The optical density OD 570 value (Abs) of each well, with background subtraction at 690 nm, was measured by means of a Tecan Infinite M200 monochromator-based multifunction microplate reader. The following formula was used to calculate the inhibition of cell growth:

Cell viability (%) = (mean Abs value of treatment group / mean Abs value of control) × 100%

LSUCLM Imaging.

Experiment to assess NaClO uptake was performed over 1 h in the same medium supplemented with 5 μM NaClO. Before the experiments, HeLa cells were washed with PBS buffer for three times, and then the cells were incubated with 350 μg/mL hCy3-csUCNPs:Nd in PBS for 2 h at 37 °C. Cell imaging was then carried out after washing the cells with PBS. LSUCLM imaging was performed with an OLYMPUS FV1000 scanning unit. Cells loaded with hCy3-csUCNPs:Nd were excited by a CW laser at 808 nm (Connet Fiber Optics, China). UCL emission was collected at 500-560 nm and 600-700 nm.

Upconversion Luminescence Imaging In Vivo

Animal procedures were in agreement with the guidelines of the Institutional Animal Care and Use Committee. One external 0-3.5W adjustable CW 808 nm semiconductor laser was used as the excitation source, a cooled electron-mulitiplying charge-coupled device (EMCCD, Andor DU897) was used as signal collector. The arthritis was induced by injecting 50 μL λ-carrageenan (10 mg/mL, in 0.9% NaCl) into the left tibiotarsal ankles of 4-week-old mouse, and the right tibiotarsal ankles injected with the same volume of physiological saline as control group. After injection of 50μL hCy3-csUCNPs:Nd, upconversion luminescence imaging in vivo was proformed under excitation power densities of 400 mW cm^{-2}. UCL signals were collected at 530±25 nm.

Acknowledgements

The authors thank the National Basic Research Program of China (973 program 2012CB932403 and 2013CB733700), National Science Foundation of China (21201038, 21231004, and 21375024), and Shanghai Sci. Tech. Comm. (12ZR1440600) for financial support.

Notes

[a] Department of Chemistry & The State Key Laboratory of Molecular Engineering of Polymers &Institute of Biomedicine Science, Fudan University, Shanghai, 200433, P. R. China. E-mail: fengweifd@fudan.edu.cn, fyli@fudan.edu.cn

Electronic Supplementary Information (ESI) available: [details of any supplementary information available should be included here]. See DOI:10.1039/b000000x/

References

1. M. T. Sun, H. Yu, H. J. Zhu, F. Ma, S. Zhang, D. J. Huang, S. H. Wang, *Anal. Chem.*, 2014, **86**, 671-677.
2. G. H. Cheng, J. L. Fan, W. Sun, J. F. Cao, C. Hu, X. J. Peng, *Chem. Commun.*, 2014, **50**, 1018-1020.
3. T. Guo, L. Cui, J. N. Shen, R. Wang, W. P. Zhu, Y. F. Xu, X. H. Qian, *Chem. Commun.*, 2013, **49**, 1862-1864.
4. Y. Koide, Y. Urano, K. Hanaoka, T. Terai, T. Nagano, *J. Am. Chem. Soc.*, 2011, **133**, 5680-5682.
5. Q. Xu, K. A. Lee, S. Lee, K. M. Lee, W. J. Lee, J. Yoon, *J. Am. Chem. Soc.*, 2013, **135**, 9944-9949.
6. Q. A. Best, N. Sattenapally, D. J. Dyer, C. N. Scott, M. E. McCarroll, *J. Am. Chem. Soc.*, 2013, **135**, 13365-13370.
7. S. R. Liu, M. Vedamalai, S. P. Wu, *Anal. Chim. Acta.*, 2013, **800**, 71-76.
8. R. Zhang, B. Song, Z. C. Dai, Z. Q. Ye, Y. N. Xiao, Y. Liu, J. L. Yuan, *Biosens. Bioelectron.*, 2013, **50**, 1-7.
9. S. Chen, J. Lu, C. Sun, H. Ma, *Analyst*, 2010, **135**, 577-582.
10. X. Cheng, H. Jia, T. Long, J. Feng, J. Qin, Z. Li, *Chem. Commun.*, 2011, **47**, 11978-11980.
11. Z. Lou, P. Li, Q. Pan, K. Han, *Chem. Commun.*, 2013, **49**, 2445-2447.
12. F. Liu, T. Wu, J. F. Cao, H. Zhang, M. M. Hu, S. G. Sun, F. L. Song, J. L. Fan, J. Y. Wang, X. J. Peng, *Analyst*, 2013, **138**, 775-778.
13. M. Sun, H. Yu, H. Zhu, F. Ma, S. Zhang, D. Huang, S. Wang, *Anal. Chem.*, 2014, **86**, 671-677.
14. F. Wang, X. G. Liu, *Chem. Soc. Rev.*, 2009, **38**, 976-989.
15. D. K. Chatteriee, A. J. Rufalhah, Y. Zhang, *Biomaterials*, 2008, **29**, 937-943.
16. J. Zhou, Z. Liu, F. Li, *Chem. Soc. Rev.*, 2012, **41**, 1323-1349.
17. N. M. Idris, Z. Q. Li, L. Ye, E. K. W. Sim, R. Mahendran, P. C. L. Ho, Y. Zhang, *Biomaterials*, 2009, **30**, 5104-5113.
18. Y. I. Park, J. H. Kim, K. T. Lee, K. S. Jeon, H. Bin Na, J. H. Yu, H. M. Kim, N. Lee, S. H. Choi, S. I. Baik, H. Kim, S. P. Park, B. J. Park, Y. W. Kim, S. H. Lee, S. Y. Yoon, I. C. Song, W. K. Moon, Y. D. Suh, T. Hyeon, *Adv. Mater.*, 2009, **21**, 4467-4471.
19. J. C. Boyer, F. Vetrone, L. A. Cuccia, J. A. Capobianco, *J. Am. Chem. Soc.*, 2006, **128**, 7444-7445.
20. N. Bogdan, F. Vetrone, G. A. Ozin, J. A. Capobianco, *Nano Lett.*, 2011, **11**, 835-840.
21. W. Feng, C. Han, F. Li, *Advanced materials*, 2013, 25, 5287-5303.
22. Q. Liu, Y. Sun, T. S. Yang, W. Feng, C. G. Li, F. Y. Li, *J. Am. Chem. Soc.*, 2011, **133**, 17122-17125.
23. M. Wang, C. C. Mi, W. X. Wang, C. H. Liu, Y. F. Wu, Z. R. Xu, C. B. Mao, S. K. Xu, *ACS Nano*, 2009, **3**, 1580-1586.
24. S. H. Nam, Y. M. Bae, Y. L. Park, J. H. Kim, H. m. Kim, J. S. Choi, K. T. Lee, T. Hyeon, Y. D. Suh, *Angew. Chem. Int. Ed.*, 2011, **50**, 6093-6097.
25. Q. Liu, W. Feng, T. S. Yang, T. Yi, F. Y. Li, *Nat. Protoc.*, 2013, **8**, 2033-2044.
26. Achatz, Daniela E.; Ali, Reham; Wolfbeis, Otto S. Topics in Current Chemistry (2011), 300, 29-50. Language: English, Database: CAPLUS, DOI: 10.1007/128_2010_98.
27. S. M. Saleh, R. Ali, O. S. Wolfbeis, *Chem. Eur. J.*, 2011, **17**, 14611-14617.
28. Q. Liu, J. J. Peng, L. N. Sun, F. Y. Li, *ACS Nano*, 2011, **5**, 8040-8048.
29. L. M. Yao, J. Zhou, J. L. Liu, W. Feng, F. Y. Li, *Adv. Funct. Mater.*, 2012, **22**, 2667-2672.
30. Y. Liu, M. Chen, T. Y. Cao, Y. Sun, C. Y. Li, Q. Liu, T. S. Yang, L. M. Yao, W. Feng, F. Y. Li, *J. Am. Chem. Soc.*, 2013, **135**, 9869-9876.
31. Y. Zhou, W. Pei, C. Wang, J. Zhu, J. Wu, Q. Yan, L. Huang, W. Huang, C. Yao, J. S. Loo, Q. Zhang, *Small*, 2014, **10**, 3560-3567.
32. M. Kumar, P. Zhang, *Langmui*r, 2009, **25**, 6024-6027.
33. S. Jiang, Y. Zhang, *Langmuir*, 2010, **26**, 6689-6694.
34. T. Soukka, T. Rantanen, K. Kuningas, *Ann. Ny. Acad. Sci.*, 2008, **1130**, 188-200.
35. H. S. Mader, O. S. Wolfbeis, *Anal. Chem.*, 2010, **82**, 5002-5004.
36. D. E. Achatz, R. J. Meier, L. H. Fischer, O. S. Wolfbeis, *Angew. Chem., Int. Ed.* 2011, **50**, 260-263.
37. R. R. Deng, X. J. Xie, M. Vendrell, Y. T. Chang, X. G. Liu, *J. Am. Chem. Soc.* 2011, **133**, 20168-20171.
38. R. Ali, S. M. Saleh, R. J. Meier, H. A. Azab, I. I. Abdelgawad, O. S. Wolfbeis, *Sensor Actuat B-Chem* 2010, **150**, 126-131.
39. Q. Q. Zhan, J. Qian, H. J. Liang, G. Somesfalean, D. Wang, S. L. He, Z. G. Zhang, S. Andersson-Engels, *Acs Nano* 2011, **5**, 3744-3757.
40. Y. F. Wang, G. Y. Liu, L. D. Sun, J. W. Xiao, J. C. Zhou, C. H. Yan, *Acs Nano* 2013, **7**, 7200-7206.
41. Y. Zhong, G. Tian, Z. Gu, Y. Yang, L. Gu, Y. Zhao, Y. Ma, J. Yao, *Advanced materials* 2014, **26**, 2831-2837.
42. X. M. Li, R. Wang, F. Zhang, L. Zhou, D. K. Shen, C. Yao, D. Y. Zhao, *Sci. Rep.* 2013, **3**, 1-7.
43. X. J. Xie, N. Y. Gao, R. R. Deng, Q. Sun, Q. H. Xu, X. G. Liu, *J. Am. Chem. Soc.* 2013, **135**, 12608-12611.
44. B. N. G. Giepmans, S. R. Adams, M. H. Ellisman, R. Y. *Tsien, Science* 2006, **312**, 217-224.
45. D. Oushiki, H. Kojima, T. Terai, M. Arita, K. Hanaoka, Y. Urano, T. Nagano, *J. Am. Chem. Soc.* 2010, **132**, 2795-2801.
46. F. Wang, R. R. Deng, J. Wang, Q. X. Wang, Y. Han, H. M. Zhu, X. Y. Chen, X. G. Liu, *Nat. Mater.* 2011, **10**, 968-973.
47. Z. Zhang, S. Achilefu, *Org. Lett.*, 2004, **6**, 2067-2070.
48. H. S. Qian, Y. Zhang, *Langmuir*, 2008, **24**, 12123-12125.
49. Z. Q. Hu, J. H. Zhu, Y. Y. Gu, W. Z. Hu, M. Li and Y. Jiang, *Microchimica Acta*, 2014, **181**, 1401-1406.
50. L. Z. Gai, J. Mack, H. Liu, Z. Xu, H. Lu and Z. F. Li, *Sensors and Actuators B-Chemical*, 2013, **182**, 1-6.
51. X. J. Wu, Z. Li, L. Yang, J. H.Han and S. F. Han, *Chemical Science*, 2013, **4**, 460-467.

52. Z. R. Lou, P. Li, P. Song and K. L. Han, *Analyst*, 2013, **138**, 6291-6295.
53. F. Ma, M. Sun, K. Zhang, Y. Zhang, H. Zhu, L. Wu, D. Huang and S. Wang, *RSC Advances*, 2014, **4**, 59961-59964.

